Impact of medium-range order on the glass transition in liquid Ni-Si alloys

Y. J. Lü[1,2,*] and P. Entel[1]

[1]*Faculty of Physics and Center for Nanointegration, CeNIDE, University of Duisburg-Essen, 47048 Duisburg, Germany*
[2]*Key Laboratory of Cluster Science, Ministry of Education of China, Department of Physics, Beijing Institute of Technology, Beijing 100081, P. R. China*

We study the thermophysical properties and structure of liquid Ni-Si alloys using molecular dynamics simulations. The liquid Ni-5% and 10%Si alloys crystallize to form the face-centered cubic (Ni) at 900 and 850 K, respectively, and the glass transitions take place in Ni-20% and 25%Si alloys at about 700 K. The temperature-dependent self-diffusion coefficients and viscosities exhibit more pronounced non-Arrhenius behavior with the increase of Si content before phase transitions, indicating the enhanced glass-forming ability. These appearances of thermodynamic properties and phase transitions are found to closely relate to the medium-range order clusters with the defective face-centered cubic structure characterized by both local translational and orientational order. This locally ordered structure tends to be destroyed by the addition of more Si atoms, resulting in a delay of nucleation and even glass transition instead.

I. INTRODUCTION

The phenomenon that in liquids the disordered and liquid state can be preserved below the melting point instead of crystallization is known as supercooling. The liquid-solid phase transition of supercooled systems has the characteristic of a nonequilibrium thermodynamic process, and there remain many open questions even now. As the most common liquid-solid phase transition, the crystallization is initiated by nucleation. The classical nucleation theory (CNT) points out that the crystal phase is directly transformed from liquids,[1,2] and this process is determined by the competition between the bulk-free energy decrease due to the formation of the new crystal phase and the interfacial free energy increase associated with the crystal-liquid interface. In the framework of CNT, the thermodynamically most-stable crystal phase will preferentially nucleate. However, the quantitative comparisons of nucleation processes between some numerical simulations and experiments show a large discrepancy. Auer and Frenkel examined the crystal nucleation of hard-sphere colloids within the CNT using numerical simulations.[3,4] They found that the calculated nucleation barrier is considerably larger than experimental values, and accordingly the nucleation rate is much smaller. In recent molecular dynamics simulations, Kawasaki and Tanaka attempted to solve this discrepancy.[5] They revealed that there is a transient random hexagonal close packing (rhcp) structure in hard-sphere liquids before crystal nucleation, and the critical nucleus will preferentially form in such medium-range order environment due to wetting effect, which lowers the nucleation barrier significantly and thus promotes the nucleation rate. In fact, the description of the non-classical nucleation behavior can be traced back to the "step rule" of Ostwald more than one century ago.[6] In his model, the crystal phase whose free energy is closest to the liquid phase will nucleate first rather than the most stable one. Furthermore, the early theoretical analyses based on the Landau theory argued that the nucleation of a body-centered cubic (bcc) phase is favored in simple liquids on the condition that a weak first-order phase transition occurs.[7] These theoretical predictions are frequently validated by the numerical simulations of

Lennard-Jones (LJ) systems at moderate supercooling,[8–11] in which the most stable face-centered cubic (fcc) phase does not form directly in supercooled liquids but via a precrystallization regime characterized by the formation of a metastable bcc nucleus. Similar experimental evidence is also found in the rapid solidification of Fe-Ni alloys.[12]

The locally ordered structure of liquids, especially super-cooled liquids, is of importance in understanding crystallization and glass transition. Cluster with the short-range order (SRO) such as icosahedron is considered a basic structural unit in metastable liquids and amorphous solids.[13–15] These locally favored structures can not fill the whole geometrical space and are regarded as the origin of frustration against crystallization,[16–18] whereas it is insufficient to describe the glass transition. Recent work extends the local order range from the nearest-neighbor distance to the second- and even third-nearest-neighbor distance, known as the medium-range order (MRO), in order to study the dynamics during the glass transition. The numerical simulations demonstrate that the frustration induced by MRO in two-dimensional liquids is directly responsible for the dynamic heterogeneity, resulting in the slow dynamics.[19,20] Up to now, the understanding of MRO remains controversial, though several structural models have been proposed. One of most interesting issues focuses on how the locally ordered clusters are connected to fill three-dimensional space. In the packing model, the clusters with local fcc or icosahedral order are supposed to be densely packed to form a configuration of overlapping clusters by sharing face, edge, and vertex.[21,22] The structural packing fails to be held beyond the length scale of a few clusters due to the fivefold symmetry favored by local order structures or chemical disorder. Ma *et al.* introduced the idea of fractal into describing the cluster connection over the MRO.[23] They showed that the packed clusters are connected via a fractal network with reduced dimensionality ($D_f = 2.31$) in metallic glasses. Different from the cluster packing models mentioned above, Liu *et al.* proposed a global packing model for supercooled metals and metallic glasses.[24] They represented the MRO structure as a combination of spherical periodic order

and local translational symmetry. The atomic arrangement within the MRO prefers the densely packed positions in fcc or hexagonal close packing (hcp) lattices. Corresponding to the radial distribution function (RDF) curves, the position ratios of the second, third, fourth peaks to the nearest-neighboring distance follow the sequence of $\sqrt{3}, \sqrt{4}, \sqrt{7}\ldots$. This model attempts to account for the splitting of the second peak in RDF curves of deeply supercooled liquids and metallic glasses.

Compared with the metallic systems, the atomic structures in liquid Si and Ge show more complicated. X-ray diffraction measurements find that the ratio of the second peak to the first peak in the RDF curves of liquid Si and Ge is 1.5, which is smaller than the value of 1.9 for most liquid metals; moreover, their bond angles are close to $109.5°$.[25] These facts suggest that there exists a large number of tetrahedral clusters, resulting in a certain degree of covalency even in the liquid state. It is noteworthy that the tendency of Si-Si covalent bond is also observed in the Si-rich transition metal (TM) alloys. Neutron diffraction experiments have confirmed the existence of the characteristic atomic separation and bond angle of Si-Si bonds in liquid $NiSi_2$ alloys.[26] On the other hand, there are plenty of intermetallic compounds found in TM-Si alloys. The locally ordered structures in liquids are believed to form with the similar stoichiometry and atomic arrangement as intermetallic phases. Despite these arguments, the exact description of the atomic configuration of liquid TM-Si alloys is still unavailable. We note that the MRO structural models mentioned above are developed based on the experimental or simulated results of TM-based amorphous alloys, in which the semiconductor element such as Si is rarely involved. Therefore, strictly speaking, it is inappropriate to apply these models to the TM-Si disordered systems, and we need a new theoretical model to describe the locally ordered structure in TM-Si alloys. In this paper, we study the thermodynamic properties and structural characteristics of liquid Ni-Si alloys during the quenching processes using molecular dynamics simulations. We intend to clarify the characteristics of the MRO in Ni-Si alloys as well as its effect on phase transitions.

The paper is organized as follows. In Sec. II , we show the simulation details and the main structural analysis methods. The results of thermophysical properties and structural analyses are presented in Sec. III . Sec. IV summarizes the main conclusions of this study.

II. METHODS

A. Molecular dynamics simulations

The present investigations are implemented using molecular dynamics simulations. We adopt the modified embedded atom method (MEAM) potential in the simulations. The MEAM potential was first proposed by Baskes *et al.* by modifying the embedded atom method (EAM) based on the density functional theory.[27,28] In the MEAM, the total energy of a system is approximated as a sum of the pairwise interaction and the embedding energy as a function of background electron density taking the bonding directionality into consideration. Baskes *et al.* attempted to reproduce the bulk properties and surface phenomena of various fcc, bcc, hcp, diamond materials, and even gaseous elements using a common

formalism.[27,28] For liquid systems, the MEAM potential shows a good application provided appropriate parameters and functional forms. The structure, melting point, and transport coefficients of liquid nickel reproduced by the MEAM potential,[29,30] for example, exhibits reasonable agreement with the experimental measurements. More importantly, the MEAM potential has been proved to be capable of effectively describing the bonding characteristic of semiconductors and their alloys. Therefore, for the TM-semiconductor systems, the MEAM is preferred. In our study, the potential parameters of Ni-Si alloys are referred to the work of Baskes *et al.* that is initially used to investigate the interface between silicon substrate and nickel thin film.[31] The C_{min} parameter in the screening function of the MEAM is chosen as 0.8 according to the suggestion of Cherne *et al.*[29] All calculations are carried out using the LAMMPS code package.[32]

The simulations are performed in the constant particle number, pressure, temperature (NPT) ensemble with $N = 13500$ atoms. Four simulated systems with the compositions of 5%, 10%, 20%, and 25% Si are prepared. The systems are first equilibrated at 2000 K for 1.5 ns, and then quenched gradually to 500 K with the average cooling rate of 4.2×10^{10} K/s to wait for the occurrence of crystallization or glass transition. The pressure is kept at zero, and the systems are sampled per 50 K for 1.2 ns. The Nosé and Hoover thermostat introduced by Melchionna is used in the simulations.[33] The periodic boundary conditions are applied in three coordinate directions, and the time step is 1 fs.

B. Structural analysis methods

The study on structural evolution during nucleation requires the effective identification of crystal particles from the liquid environment. One of the methods is the solidlike criterion.[34,35] First, a complex vector $q_{lm}(i)$ of particle i is defined as

$$q_{lm}(i) = \frac{1}{N_b(i)} \sum_{j=1}^{N_b(i)} Y_{lm}(\mathbf{r}_{ij}), \qquad (1)$$

where $N_b(i)$ is the number of the nearest neighbors of particle i, $\mathbf{r}_{ij}$ is the vector from particle i to particle j, and $Y_{lm}(\mathbf{r}_{ij})$ are spherical harmonics. Lechner and Dellago proposed an average version about the vector $\bar{q}_{lm}(i)$,[36]

$$\bar{q}_{lm}(i) = \frac{1}{\tilde{N}_b(i)} \sum_{k=0}^{\tilde{N}_b(i)} q_{lm}(k), \qquad (2)$$

where $\tilde{N}_b(i)$ includes all the neighbors of particle i, and $k = 0$ denotes the particle i itself. Thus $\bar{q}_{lm}(i)$ averages the $q_{lm}(i)$ associated with particle i and its neighbors, and in fact it covers the structural information of both the first and second shells. Then, use the normalized component vector $\tilde{q}_{6m}(i)$,

$$\tilde{q}_{6m}(i) = \frac{\bar{q}_{6m}(i)}{\left[\sum_{m=-6}^{6} |\bar{q}_{6m}(i)|^2 \right]^{1/2}}, \qquad (3)$$

to define the vector of $\mathbf{q}_6$ neighboring particle i and j,

$$\mathbf{q}_6(i) \cdot \mathbf{q}_6(j) = \sum_{m=-6}^{6} \tilde{q}_{6m}(i)\tilde{q}_{6m}(j)^*. \qquad (4)$$

If the dot product is larger than a certain threshold, typically 0.5, two particles i and j are defined to be connected. If the number of connections of particle i exceeds a threshold value, 7 in our case of Ni-Si liquids, the particle i is identified as solidlike. This method can effectively distinguish between solidlike and liquidlike particles and be used to globally analyze the nucleation process in liquids, but it can not judge a special crystal structure.

Another method is to utilize the local bond order parameter that is defined as[37]

$$\bar{q}_l(i) = \sqrt{\frac{4\pi}{2l+1} \sum_{m=-l}^{m=l} |\bar{q}_{lm}(i)|^2}. \quad (5)$$

These parameters are sensitive to different crystal structures. In particular, $\bar{q}_4$ and $\bar{q}_6$ are frequently applied to the discrimination between cubic and hexagonal structures. At first, we construct a reference $\bar{q}_4 - \bar{q}_6$ frame that provides the distributions of $\bar{q}_4$ and $\bar{q}_6$ for normal liquid and various perfect crystal structures and then plot the $\bar{q}_4 - \bar{q}_6$ plane of concerned systems. By comparing the $\bar{q}_4 - \bar{q}_6$ plane with the reference frame, the structural information can be acquired.

It is noted that this method seems more feasible for a single-component LJ system, and may be rather difficult to apply to a multicomponent realistic system such as alloys because of the difficulty in constructing the reference frame. Therefore, the common neighbor analysis (CNA) method[38] is used jointly to describe the structural evolution through crystallization. In CNA, each particle pair is characterized by four indices that represent the topological relation with their neighboring particles. Every crystal structure has its characteristic indices, and therefore we can determine qualitatively the crystal structure by the distribution of these indices.

C. Transport properties

The self-diffusion coefficient and the viscosity are calculated during the quenching process. The self-diffusion coefficient is obtained by the long-time limit of the mean-squared displacement (MSD),

$$D_i = \frac{1}{6N_i} \lim_{t\to\infty} \sum_{j=1}^{N_i} \frac{1}{t} \langle |\mathbf{r}_j^{(i)}(t) - \mathbf{r}_j^{(i)}(0)|^2 \rangle, \quad (6)$$

where $\mathbf{r}_j^{(i)}(t)$ and $\mathbf{r}_j^{(i)}(0)$ are the positions of particle j of species i at time t and 0, respectively, and N_i is the particle number of species i. In the simulations, the atomic configuration is recorded every 2 ps, and MSD is averaged statistically for 100 measurements with the time interval of 200 ps. Then the self-diffusion coefficient is achieved from the convergence of Eq. (6) to asymptotic behavior.

The equilibrium MD method is employed in the calculation of viscosity.[39] Based on the integrated autocorrelation function of the pressure tensor, the Green-Kubo relation defines the viscosity, η as

$$\eta = \frac{V}{k_B T} \int_0^\infty \left\langle \sum_{\alpha \neq \beta} P_{\alpha\beta}(t) P_{\alpha\beta}(0) \right\rangle dt, \quad (7)$$
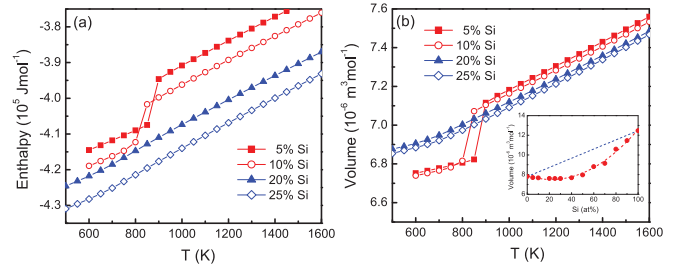

FIG. 1. (Color online) Thermodynamic properties of liquid Ni-Si alloys as a function temperature, (a) enthalpy, and (b) molar volume. The inset shows the composition dependence of molar volume.

where

$$P_{\alpha\beta} = \sum_{j=1}^{N} \left(\frac{p_{\alpha j} p_{\beta j}}{m_j} + r_{j\alpha} F_{j\beta} \right) \quad (\alpha,\beta = x,y,z). \quad (8)$$

$P_{\alpha\beta}$ is the off-diagonal element ($\alpha \neq \beta$) of the pressure tensor. $p_{\alpha j}$ and $p_{\beta j}$ denote the momenta of the jth particle along α and β directions, $r_{j\alpha}$ and $F_{j\beta}$ are the components of the position and force on the jth particle, respectively. The pressure tensors are output every 2 fs. Since the decay of the autocorrelation function of the pressure tensor becomes slower as the temperature decreases, the time used in the integration of Eq. (7) is prolonged from 2 to 20 ps, when the systems are cooled, approaching the phase transitions. The final viscosity is produced by the average over 1000 measurements.

III. RESULTS AND DISCUSSION

A. Thermodynamic and transport properties

The enthalpies of Ni-5%, 10%, 20%, and 25% Si during the quenching processes are shown in Fig. 1(a). The values approximately decrease linearly with decreasing temperature in the liquid regime. From the derivation of enthalpy with respect to temperature, the specific heat of the liquid alloys is obtained. Compared with the available experimental value of 39.54 J·mol^{-1}K^{-1} for Ni-9.9%Si above 1400 K,[40] the present specific heat of Ni-10%Si, 34.14 J·mol^{-1}K^{-1} shows a reasonable agreement. For Ni-5% and 10%Si alloys, the temperature-dependent enthalpies are found to abruptly drop below 900 and 850 K, respectively, implying the occurrences of crystallization, but the similar changes are not observed in the quenching processes of Ni-20% and 25%Si alloys. Instead, two turning points appear near 700 K, which is more obvious in the molar volume-temperature curves as shown in Fig. 1(b). Due to the continuous decrease of enthalpy and free volume featuring the glass transition, we conclude that glass transitions take place when the liquid 20%, 25%Si alloys are cooled approaching to 700 K. Both enthalpy and molar volume of liquid Ni-Si systems show remarkable concentration dependence, decreasing with increasing Si content. The experimental molar volumes of liquid Ni and Si at 1800 K are 7.51×10^{-6} and 11.29×10^{-6} m^{3}mol^{-1}, respectively.[41] We calculate molar volumes in the whole concentration range at 1800 K, and the values of pure Ni and Si are 7.80×10^{-6} and 12.46×10^{-6} m^{3}mol^{-1}, which agrees with the experimental measurements. More importantly, its concentration dependence does not obey a linear relation [inset in Fig. 1(b)]. The molar
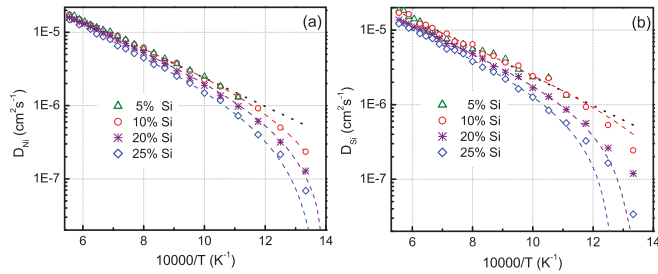
FIG. 2. (Color online) Self-diffusioncoefficients of liquid Ni-Si alloys. (a) and (b) show the self-diffusion coefficients of Ni and Si, respectively. The dotted lines are the Arrhenius fit and dashed lines are power-law fits.
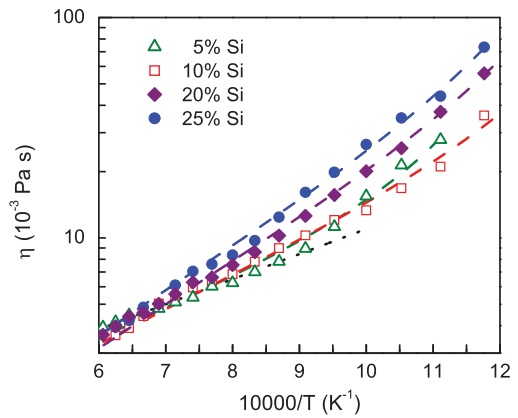

FIG. 3. (Color online) Viscosity of liquid Ni-Si alloys versus inverse temperature. The dotted line results from a fit to the Arrhenius relation for Ni-5% Si and the dashed lines result from a fit to the power law for Ni-5%, 10%, 20%, and 25% Si.

volume tends to decrease when Si content increases. The excess volume, defined as the volume difference between ideal solutions and real alloys, reaches its maximum at 30%Si, and then the molar volume begins to increase with concentration. Obviously, Ni-Si melts cannot be described by the ideal solution model. Similar strong mixing effect of liquid alloys is also observed in other alloy melts such as Fe-Cu alloys,[42] implying the closer interaction between the two components. Besides the mixing effect of thermodynamic properties, introducing more Si atoms causes the change of phase transition types from crystallization to glass transition.

Transport properties are important parameters for scaling the liquid-solid phase transition, especially the glass transition. We calculate the self-diffusion coefficients and the viscosities of the four alloys as a function of temperature. Figures 2(a) and 2(b) exhibit the self-diffusion coefficients of Ni and Si versus inverse temperature ($1/T$). The simulations indicate that the self-diffusion of both Ni and Si atoms is slowed down as the concentration increases. In general, the temperature-dependent diffusion coefficients of liquids follow the Arrhenius relation,$D = D_0 \exp(-Q/RT)$, where Q is the diffusion activation energy, D_0 is the pre-exponential factor, and R is the gas constant. This relation can well describe the temperature behavior of Ni-5%Si upon crystallization but obviously deviates from the simulated results of Ni-10%Si in the low-temperature region before crystallization. The non-Arrhenius behavior becomes more significant for 20% and 25%Si alloys, in particular when approaching the glass transitions. The dependence of dynamic properties on the Arrhenius law is often used to distinguish "strong" from "fragile" liquids.[43,44] The more highly non-Arrhenius the dynamic properties are, the more fragile the liquids are. Thus, the fragility of liquid Ni-Si alloys is enhanced with the increase of Si concentration. The other transport property considered here is viscosity. Figure 3 shows the viscosity versus inverse temperature. Similar to the self-diffusion coefficients, the T-dependence of viscosity of the four alloys is characterized by non-Arrhenius behavior. Here, we use a power law, $\eta = \eta_0(T/T_0 - 1)^\gamma$ to fit the simulated data, which is also applied in the study of dynamic behaviors of liquid silicon,[45] where T_0 is the divergence temperature. For the two glass-forming systems, Ni-20%Si and Ni-25%Si, the fitting yields the divergence temperatures $T_0 = 661$ and 675 K with the exponents $\gamma = -1.71$ and -1.73, respectively. These temperatures are very close to the glass transition temperatures predicted by enthalpy and molar volume. Furthermore, we note

that the divergence temperature of Ni-25%Si alloy is smaller than Ni-20%Si, indicating the stronger glass-forming ability and fragile behavior for the former.

Both thermodynamic and transport properties have demonstrated the enhancement of glass-forming ability by the increase of Si content. In order to further understand the effect of Si atoms on the phase transition, it is necessary to analyze the structural characteristics of liquids.

B. Crystallization process

In the Ni-Si equilibrium phase diagram, the liquid Ni-5%Si and Ni-10%Si alloys are solidified to fcc (Ni) solid solutions. According to the prediction of the CNT, the fcc-ordered critical nucleus directly segregates from the disordered melts. In order to monitor the crystallization process, we use the local bond order parameter to scale the ordering degree through crystallization. For the binary alloys, constructing the reference frame of $\bar{q}_4 - \bar{q}_6$ plane becomes obscured in contrast to simple LJ liquids because it is difficult to determine various underlying crystal phases during the cooling and crystallization. However, we can quantitatively judge the structural constituents using CNA method at first. In the calculations, only the atoms in the nearest-neighboring distance are involved. In the whole liquid regime, the dominant bond pairs are 1422 and 1431 (~10%), and then 1421 pair sharply rises (~70%) when the crystallization begins, as shown in Fig. 4. The 1421 pair is the major characteristic pair in bulk fcc crystal, while the 1422 pair is contained in the bulk hcp crystal. The 1431 pair is mainly observed in liquids or amorphous systems, but it is not excluded that some 1421 pairs are mistaken as 1431 pairs when using the CNA method. We note that the fraction of the 1551 pair, the main bond pair composing the icosahedral cluster, is much lower. The icosahedral cluster is the primary locally ordered structure in many supercooled liquids and glass metals, which plays a crucial role in suppressing nucleation and promoting the formation of glass. Its absence in our work implies a different formation mechanism of Ni-Si metallic glasses. The CNA results verify that the crystal structure obtained in the present simulations is an fcc order, consistent with the equilibrium phase diagram.
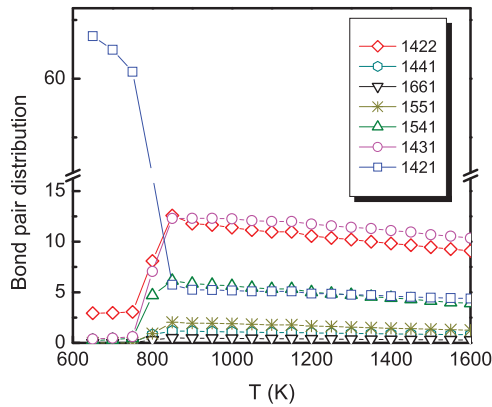
FIG. 4. (Color online) Bond pair distribution of Ni-10%Si as a function of temperature from the common neighbor analysis method.

With the aid of the structural information above, the crystallization of Ni-10%Si alloy is plotted in the $\bar{q}_4 - \bar{q}_6$ planes. A reference frame, including the normal liquid state and perfect fcc crystal, is given in Fig. 5(a). Due to thermal fluctuations, the order parameters of the homogeneous liquid and fcc crystal show a distribution. From Figs. 5(b) to 5(d), the Ni-10%Si alloy experiences a process from nucleation to the accomplishment of crystallization below 850 K. It is found that $\bar{q}_6$ obviously jumps to a high-value region (>0.35) after crystallization, whereas $\bar{q}_4$ disperses onto a wider range through the process. Therefore, we choose $\bar{q}_6$ equal to 0.35 as a threshold to distinguish liquidlike and fcc-like atoms. The three-dimensional structural evolution associated with $\bar{q}_6$ is shown in Fig. 6. It distinctly traces the process from the formation of stable fcc nucleus to the finish of crystallization. We examine the
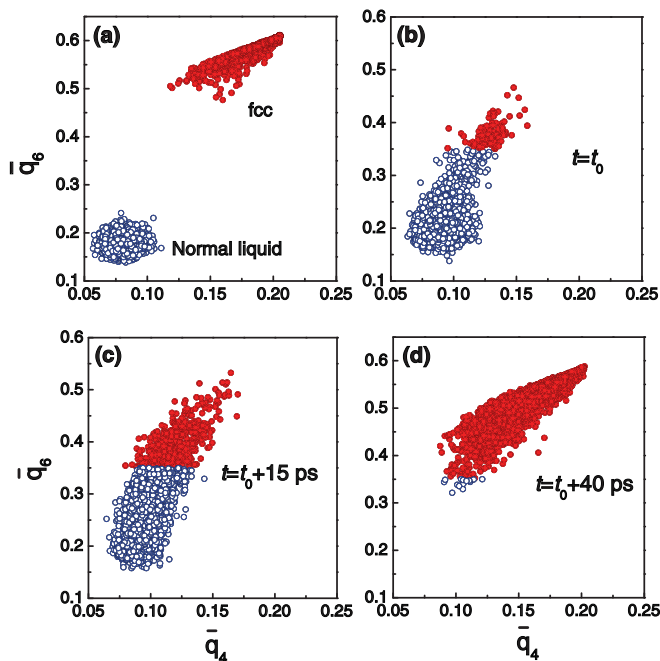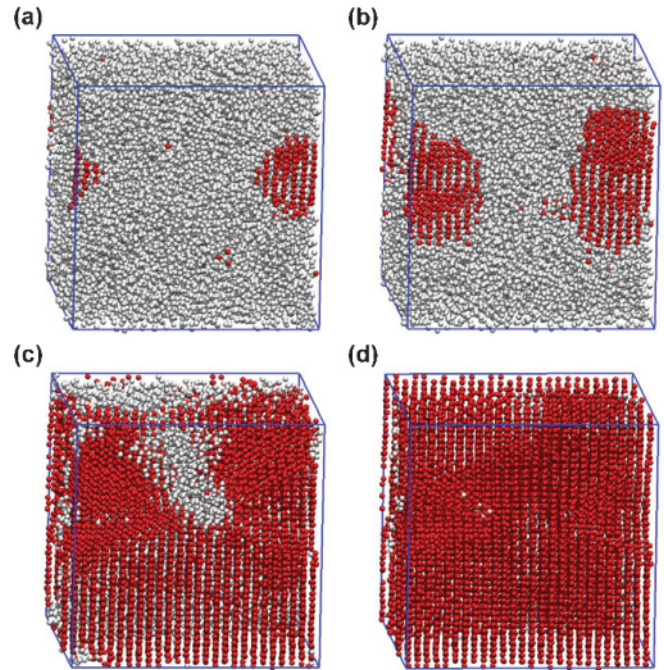

FIG. 6. (Color online) The crystallization process of Ni-10% Si at 850 K in three dimensions. We choose a threshold value of $\bar{q}_6 = 0.35$ to distinguish fcc ordered atoms from liquids. Light balls mark liquid atoms with $\bar{q}_6 < 0.35$ and dark balls are fcc ordered atoms with $\bar{q}_6 > 0.35$.

composition of nuclei in both 10% and 5% Si alloys and find only Ni atoms take part in forming the stable nuclei and no Si atoms are involved. Obviously, the Si-centered clusters are not the effective locations to stimulate nucleation. It can be speculated that the effective nucleating region shrinks with the addition of more Si atoms, leading to the decrease of nucleation probability and the enhancement of glass-forming ability.

From the CNA results, the SRO structure in the supercooled liquids before nucleation is characterized by hcp order. A similar process is also produced in the simulations of colloid systems.[5] The emergence of the hcp order is interpreted as a result of reduction of the interfacial energy due to the wetting of the fcc nucleus to hcp clusters, thus lowering the free-energy barrier of nucleation. This agrees with the description of Ostwald's "step rule" and is believed to contribute to solve the discrepancy between experimental measurements and numerical calculations of the nucleation rate. However, we note that quite a few 1422 bond pairs are conserved after crystallization of Ni-5%Si alloy. Compared with the atomic configuration of Ni-10%Si alloy, we find the apparent grain boundary formed in Ni-5%Si alloy, where the atomic arrangement displays more disordered. Therefore, it is inferred that 1422 bond pairs obtained in present simulations likely reflect a kind of defective fcc rather than hcp structure.

FIG. 5. (Color online) $\bar{q}_4$-$\bar{q}_6$ plane for Ni-10% Si alloy. (a) Reference frame in the $\bar{q}_4$-$\bar{q}_6$ plane which shows the distribution of $\bar{q}_4$ and $\bar{q}_6$ of liquid Ni-10% Si at 1800 K and fcc ordered Ni-10% Si at 300 K. (b), (c) and (d) shows the crystallization process of Ni-10% Si alloy at 850 K.

C. Liquid structure and glass transition

Before the discussion of the liquid structure, we test the validity of MEAM potentials in describing the liquid structure of Ni-Si alloys. We calculate the partial structure factors of Ni-25%Si alloy in normal liquid state by integrating the partial
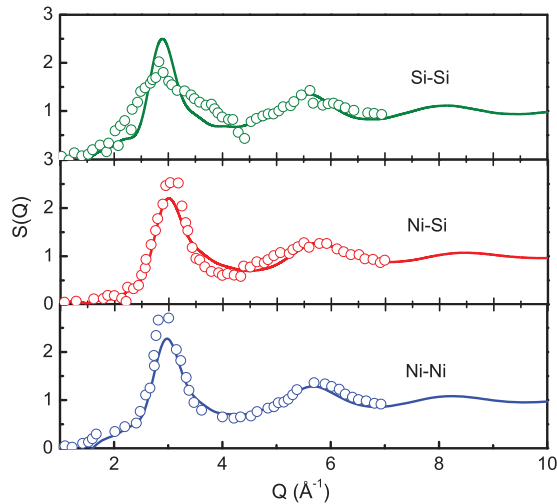
FIG. 7. (Color online) Structure factor of liquid Ni-25%Si alloy at 1800 K. Solid lines are the calculated results, and open circles are experimental measurements.

RDF $g(r)$,

$$S(Q) = 1 + \rho \int g(r) \exp(-i\mathbf{Q} \cdot \mathbf{r}) dr, \qquad (9)$$

and compare the results with the experimental measurements,[46] where ρ is the liquid density. Figure 7 shows the simulated and experimental partial structure factors of Ni-Ni, Ni-Si, and Si-Si pairs of Ni-25%Si alloy at 1800 K. The locations of the calculated first and second peaks agree well with experiments, and the amplitudes of the first peaks in experiments show a little higher than the simulations for Ni-Ni and Ni-Si pairs but lower for Si-Si pairs. The oscillation behavior at low Q reported by experiments is also confirmed by our simulations. Briefly speaking, the present MEAM

potential can reasonably describe the structural characteristics of liquid Ni-Si systems.

Figure 8 shows the partial radial distribution functions of Ni-10%Si and Ni-25%Si in high- and low-temperature liquid states ($T = 1800$ and 1000 K), crystal, and amorphous states. A pronounced characteristic in these RDF curves is the emergence of a subpeak between the first and second peaks when the liquids are cooled into the low-temperature region. The subpeak is found in all the four alloys and becomes more remarkable with decreasing temperature. It is different from the splitting of the second peak featuring some metallic glasses and suggests a new MRO structure. The subpeak develops into a crystal peak after crystallization with a right shift. For Ni-20%Si and Ni-25%Si alloys, the subpeaks are retained after glass transitions. A similar subpeak is also observed in liquid silicon. Numerical simulations show that a small peak is inclined to grow near the left side of the second peak for the supercooled and high-density silicon and disappears while the liquid-liquid phase transition (from high-density to low-density liquid silicon) occurs,[45] which suggests that the locally ordered structure is similar to that in Ni-Si alloys; moreover, such local structure is not favored by low-density liquid or amorphous Si.

The next problem we are concerned with is how to describe this MRO in Ni-Si alloys and how it affects phase transition. Recent work on the structure of metallic glasses represents the MRO in the metallic glass as a combination of spherical periodic order and translational symmetry.[24] They achieved the global structural information by calculating the position ratios between the peaks related to the MRO and the first peak in RDF curves and found that the ratio values are well consistent with the atomic arrangement in fcc crystals along the dense-packing direction. This is a simple and reasonable method to study the locally ordered structure of liquids or metallic glasses from a global viewpoint. Therefore, we use
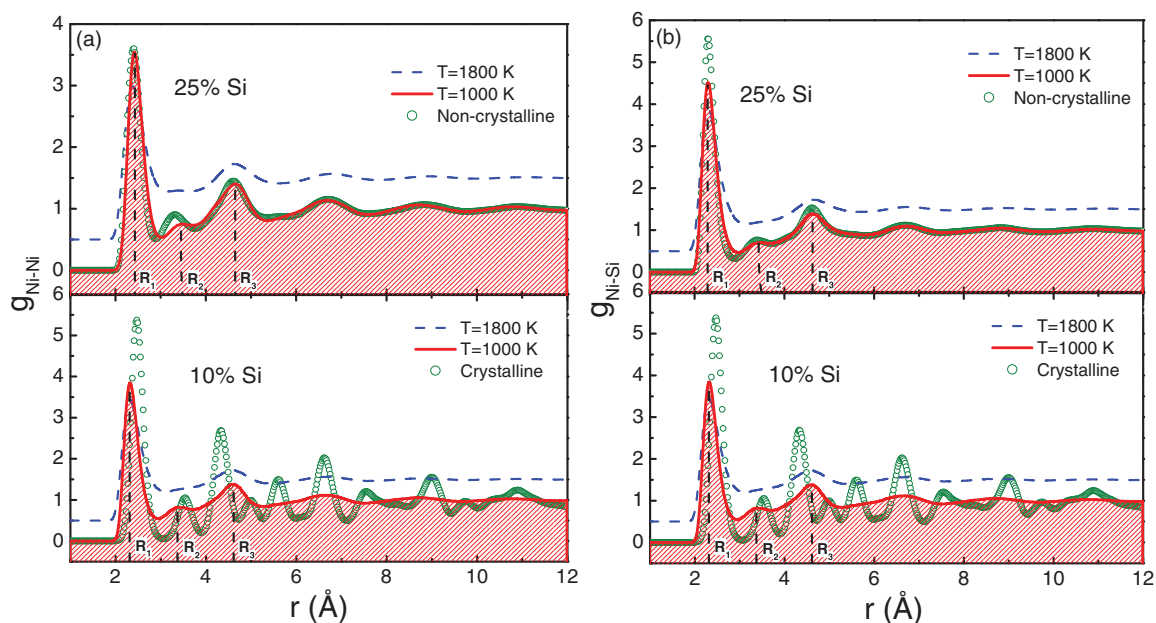

FIG. 8. (Color online) Partial radial distribution functions of Ni-10% and 25%Si (a) Ni-Ni pair and (b) Ni-Si pair. Dashed lines denote normal liquids at 1800 K, solid lines describe liquids at 1000 K, and open circles show results of crystalline or noncrystalline.

this idea to re-examine the simulated RDF. We calculate the position ratios of the second, third, and fourth peaks to the first peak for the four Ni-Si alloys (here, the subpeak is retermed as the second peak), and results are listed in Table I. The relative distances of the second, third, and fourth peaks to the first peak are close to $\sqrt{2}$ (1.414), $\sqrt{4}$ (2.000), and $\sqrt{8}$ (2.828). This sequence is not consistent with the prediction of the global packing model that represents the atomic arrangement with MRO as a one-dimensional translational order along the densely packed direction, namely following the sequence of $\sqrt{3}$, $\sqrt{4}$, $\sqrt{7}$.... We impose the calculated relative positions on the three-dimensional fcc structure, as shown in Fig. 9(a), and obviously the positions of the second, third and fourth peaks actually occupy the lattice point positions rather than along the densely packed direction. The major conclusion of the global packing model is based on the statistical analyses of the RDF results of 64 metallic glasses from experiments and simulations.[24] We examine the 64 metallic glasses and find that these samples range from Cu, Ni, and Al pure metals to Fe-, Ni-, Zr-, and Cu-based binary or multicomponent alloys, in which, however, the semiconductor element Si is rarely involved. We speculate that the difference between this work and the global packing model has arisen from different alloy types. For the alloys composed of Si element, the interaction between Si and metallic atoms often shows more strong directionality, forming complicated intermetallic compounds. These bonding characteristics affect the local structure in deeply supercooled liquids. In these ordered structures, whether the Si tetrahedral clusters form is another question that we are concerned about. We compare the present results with the structural analyses of Si-rich Ni-Si alloys, and the second-nearest distance of Si-Si pairs reaches 4.41 Å, which is larger than the characteristic atomic separation of Si-Si covalent bonds (3.70 Å),[25,26] indicating no Si-Si covalent cluster forms. A possible explanation is that the formation of such cluster largely depends on the concentration, and the Si-rich system is favored.

The global packing model proposes the concept of one-dimensional translational order, in which the orientational order is excluded, and thus the MRO clusters are absent of three-dimensional crystal periodicity.[24] Assuming that the

TABLE I. Ratios of the second, third, and fourth shells to the first shell for Ni-Ni and Ni-Si pairs.

	R_2/R_1		R_3/R_1		R_4/R_1	
Si (at%)	Ni-Ni	Ni-Si	Ni-Ni	Ni-Si	Ni-Ni	Ni-Si
5	1.421	1.456	1.931	1.968	2.784	2.841
10	1.412	1.482	1.921	1.983	2.773	2.882
20	1.402	1.470	1.932	2.003	2.807	2.902
25	1.405	1.497	1.931	2.013	2.820	2.924

orientational order is embodied in the MRO, the angle between the two vectors from the centered atom pointing to its two neighboring atoms in the first and second shells should be approximately 45°, as illustrated in Fig. 9(a). We calculate the bond angle distributions of the four Ni-Si alloys. In order to clear the effect of the MRO on the bond angle distribution, comparative computations are performed in both the first and second shells. Figure 10 shows the calculated results of Ni-10% Si and Ni-25% Si. In the distribution curve associated with the second shell, the main peak emerges near 45°, whereas it disappears in the case that only the first shell is considered. It is obvious that the angle of 45° arises from the second shell that has a preferred orientational relationship with the first shell. Globally, the characteristic of the MRO of Ni-Si alloys is not only the translational order but also the orientational symmetry. Actually, this is a kind of local three-dimensional crystal cluster similar to the fcc structure except that atoms along the densely packed direction partially lacks, namely, a defective fcc structure, which is consistent with the analyses of CNA results. Figure 9(b) shows a typical MRO cluster that clearly illustrates the position and orientation relation among atoms within the medium range. We note that a shoulder peak of 57° accompanies the main peak of 45°, and it becomes the main peak in the curve of the first shell, which is proved to be the characteristic peak of completely disordered liquids. For Ni-20% Si and Ni-25% Si alloys, the orientational order is enhanced when the glass transition occurs. In the distribution, there is no peak near 109.5°, which further confirms the conclusion that no Si covalent cluster forms in our simulations.
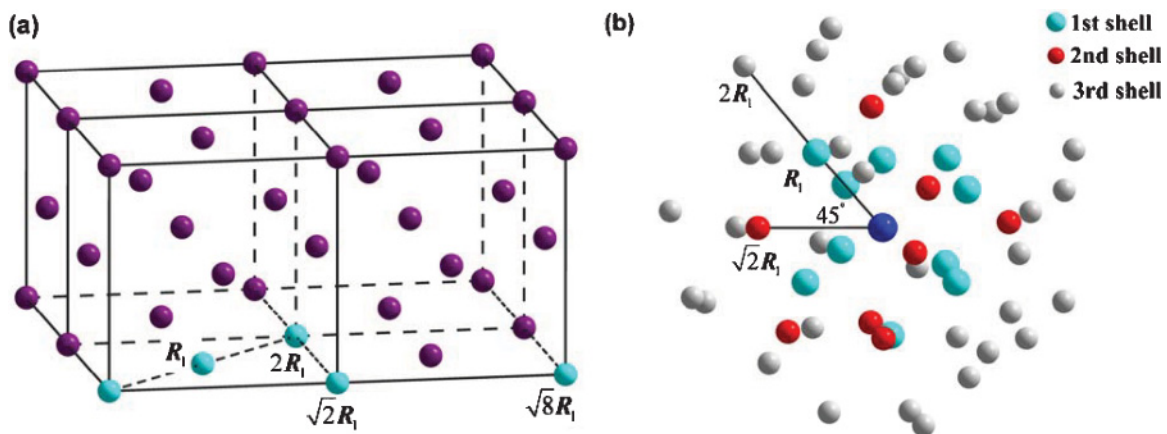

FIG. 9. (Color online) (a) The MRO structure in our simulations, which is characterized by the local transitional and orientational order. (b) shows a typical cluster of MRO of Ni-10% Si at 1200 K as it appears in the simulations.
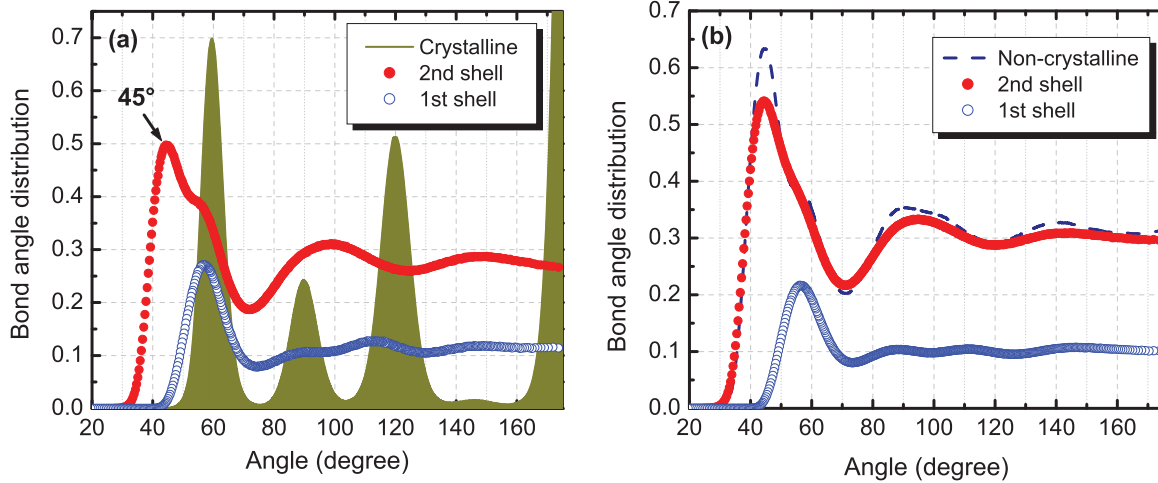
FIG. 10. (Color online) Bond angle distribution of cluster. (a) Ni-10% Si, (b) Ni-25% Si. Solid circles are results considering the second shell, and open circles are the results only in the nearest-neighbor distance. The dark region plots the bond angle distribution of the crystalline structure.

The MRO clusters have similar structure compared with the stable fcc crystal. During nucleation, they are ready to transform to fcc nuclei due to the low nucleation barrier. Therefore, the MRO in Ni-Si alloys is a transient local order structure that is beneficial for nucleation similar to the role of the rhcp structure in LJ liquids. On the other hand, in contrast to the Ni-centered clusters, the position ratios of the second peak to the first peak for the Si-centered clusters are universally larger than $\sqrt{2}$ and approach 1.5. This suggests that MRO is inclined to be degenerated in Si-centered clusters, and as a result a higher nucleation barrier has to be required to overcome the position mismatching. With the increase of Si content, the number of deformed MRO clusters increases accordingly, leading to the decrease of nucleation probability until a glass transition occurs. In order to measure directly the nucleation ability, we calculate statistically the maximum size of solid clusters as a function of temperature for the four alloys, as shown in Fig. 11. The maximum solid cluster decreases with increasing Si content at a given temperature. For Ni-5% Si and Ni-10% Si, the values increase exponentially, whereas linearly rise occurs for the Ni-20% Si and Ni-25% Si systems. The
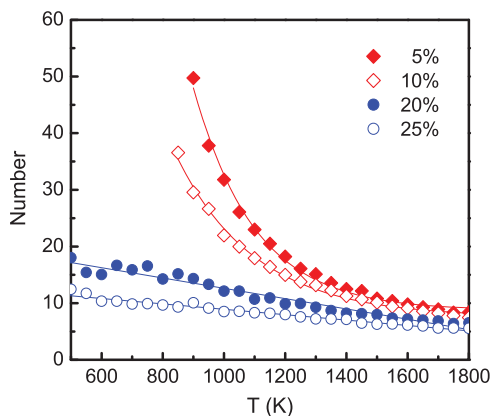
results are identical with the fact that the glass-forming ability is enhanced, while the nucleation ability is lowered from 5% to 25% Si. If the concentration further increases to 50%, our simulations exhibit a rapid crystallization at 1600 K, forming a NiSi intermetallic compound. Therefore, the above conclusion is valid in the low-concentration range.

IV. CONCLUSIONS

The present molecular dynamics simulations reveal the MRO in liquid Ni-Si alloys. Unlike the locally ordered structure in some metallic glasses, the MRO of liquid Ni-Si alloys can be described as the defective fcc structure that combines the local transitional and orientational order. Such local structure is beneficial for the formation of the critical fcc nuclei due to a smaller nucleation barrier. In the simulations, we do not observe the evidence of Si covalent clusters as those in Si-rich systems. However, the Si-centered cluster tends to lower the local symmetry by destroying the transitional order, which is capable of suppressing nucleation. As a result, the crystallization for Ni-5% and 10% Si, but the glass transition for Ni-20% and 25%Si are obtained in our simulations. The local structural evolution affects the thermodynamic and transport appearance. With the increase of Si content to 25%, the excess volume and viscosity increase, and the self-diffusion coefficients decrease. Especially, the non-Arrhenius behavior of diffusion and viscosity becomes more pronounced and the glass-forming ability is enhanced as the Si content increases. Our results give a new perspective on the order in disordered systems and are helpful to further understand the glass-forming mechanism and the structure-property relationship.

FIG. 11. (Color online) Maximum solidlike clusters of Ni-Si alloys as a function of temperature.

*Corresponding author: yongjunlv@tsinghua.edu.cn

[1] F. F. Abraham, *Homogeneous Nucleation Theory* (Academic Press, New York, 1974), p. 80.

[2] J. Frenkel, *Kinetic Theory of Liquids* (Oxford University Press, Oxford, 1946), p. 366.

[3] S. Auer and D. Frenkel, Nature **409**, 1020 (2001).

[4] S. Auer and D. Frenkel, Nature **413**, 711 (2001).

[5] T. Kawasaki and H. Tanaka, Proc. Natl. Acad. Sci. USA **107**, 14036 (2010).

[6] W. Ostwald, Z. Phys. Chem. **22**, 289 (1897).

[7] W. Klein and F. Leyvraz, Phys. Rev. Lett. **57**, 2845 (1986).

[8] W. C. Swope and H. C. Andersen, Phys. Rev. B **41**, 7042 (1990).

[9] P. R. ten Wolde, M. J. Ruiz-Montero, and D. Frenkel, Phys. Rev. Lett. **75**, 2714 (1995).

[10] P. R. ten Wolde, M. J. Ruiz-Montero, and D. Frenkel, J. Chem. Phys. **104**, 9932 (1996).

[11] P. R. ten Wolde, D. W. Oxtoby, and D. Frenkel, Phys. Rev. Lett. **81**, 3695 (1998).

[12] R. E. Cech, Trans. AIME. J. Met. **8**, 585 (1956).

[13] P. J. Steinhardt, D. R. Nelson, and M. Ronchetti, Phys. Rev. Lett. **47**, 1297 (1981).

[14] P. Wochner, C. Gutt, T. Autenrieth, T. Demmer, V. Bugaev, A. Ortiz, A. Duri, F. Zontone, G. Grübel, and H. Dosch, Proc. Natl. Acad. Sci. USA **106**, 11511 (2009).

[15] S. Torquato and Y. Jiao, Nature **460**, 876 (2009).

[16] G. Tarjus, S. A. Kivelson, Z. Nussinov, and P. Viot, J. Phys.: Condens. Matter **17**, R1143 (2005).

[17] M. Dzugutov, Phys. Rev. A **46**, R2984 (1992).

[18] J. P. Doye, D. J. Wales, F. H. Zetterling, and M. Dzugutov, J. Chem. Phys. **118**, 2792 (2003).

[19] H. Shintani and H. Tanaka, Nat. Phys. **2**, 200 (2006).

[20] T. Kawasaki, T. Araki, and H. Tanaka, Phys. Rev. Lett. **99**, 215701 (2007).

[21] D. B. Miracle, Nat. Mater. **3**, 697 (2004).

[22] H. W. Sheng, W. K. Luo, F. M. Alamgir, J. M. Bai, and E. Ma, Nature **439**, 419 (2006).

[23] D. Ma, A. D. Stoica, and X. L. Wang, Nat. Mater. **8**, 30 (2009).

[24] X. J. Liu, Y. Xu, X. Hui, Z. P. Lu, F. Li, G. L. Chen, J. Lu, and C. T. Liu, Phys. Rev. Lett. **105**, 155501 (2010).

[25] Y. Kita, J. B. Van Zytveld, Z. Morita, and T. Iida, J. Phys.: Condens. Matter **6**, 811 (1994).

[26] S. Gruner, J. Marczinke, L. Hennet, W. Hoyer, and G. J. Cuello, J. Phys.: Condens. Matter **21**, 385403 (2009).

[27] M. I. Baskes, Phys. Rev. B **46**, 2727 (1992).

[28] M. I. Baskes, J. S. Nelson, and A. F. Wright, Phys. Rev. B **40**, 6085 (1989).

[29] F. J. Cherne, M. I. Baskes, and P. A. Deymier, Phys. Rev. B **65**, 024209 (2001).

[30] F. J. Cherne, M. I. Baskes, R. B. Schwarz, S. G. Srinivasan, and W. Klein, J. Phys.: Condens. Matter **1**, 0302491 (2003).

[31] M. I. Baskes, J. E. Angelo, and C. L. Bisson, Modelling Simul. Mater. Sci. Eng. **2**, 505 (1994).

[32] S. Plimpton, J. Comput. Phys. **117**, 1 (1995).

[33] S. Melchionna, G. Ciccotti, and B. L. Holian, Mol. Phys. **78**, 533 (1993).

[34] P. J. Steinhardt, D. R. Nelson, and M. Ronchetti, Phys. Rev. B **28**, 784 (1983).

[35] P. R. ten Wolde, M. J. Ruiz-Montero, and D. Frenkel, J. Chem. Phys. **104**, 9932 (1996).

[36] W. Lechner and C. Dellago, J. Chem. Phys. **129**, 114707 (2008).

[37] C. Desgranges and J. Delhommelle, Phys. Rev. B **77**, 054201 (2008).

[38] J. D. Honeycutt and A. C. Andersen, J. Phys. Chem. **91**, 4950 (1987).

[39] M. P. Allen and D. J. Tidesley, *Computer Simulation of Liquids* (Clarendon, Oxford, 1989), p. 60.

[40] H. P. Wang and B. Wei, Phil. Mag. Lett. **88**, 813 (2008).

[41] E. A. Brandes and G. B. Brook, editors, *Smithells Metals Reference Book* (Butterworth-Heinemann, Oxford, United Kingdom, 1992), p. 14.

[42] I. Egry and J. Brillo, J. Chem. Eng. Data **54**, 2347(2009).

[43] C. A. Angell, J. Non-Cryst. Solids **131-133**, 13 (1991).

[44] C. A. Angell, Science **267**, 1924 (1995).

[45] S. Sastry and C. A. Angell, Nat. Mater. **2**, 739 (2003).

[46] Y. Wased and S. Tamaki, Philos. Mag. **32**, 951 (1975).